Physiological Reports

Open Access

Physiological Reports ISSN 2051-817X

ORIGINAL RESEARCH

Hyperpolarized ^{3}He magnetic resonance imaging ventilation defects in asthma: relationship to airway mechanics

Del Leary[1], Sarah Svenningsen[2,3], Fumin Guo[2,4], Swati Bhatawadekar[5], Grace Parraga[2,3,4] & Geoffrey N.Maksym[6]

1 Department of Environmental and Radiological Health Sciences, Colorado State University, Fort Collins, Colorado
2 Robarts Research Institute, The University of Western Ontario, London, Canada
3 Department of Medical Biophysics,The University of Western Ontario, London, Canada
4 Graduate Program in Biomedical Engineering, The University of Western Ontario, London, Canada
5 University Health Network-Toronto Rehabilitation Institute, Toronto, Canada
6 School of Biomedical Engineering, Dalhousie University, Halifax, Canada

Keywords
FEV_1, heterogeneity, hyperpolarized MRI, lung impedance, ventilation defects.

Correspondence
Geoffrey N. Maksym, Dalhousie University
5981 University Ave, PO Box 15000
Halifax, Nova Scotia, Canada B3H 4R2.
Tel: 902-494-2624
Fax: 902-494-6621
E-mail: gmaksym@dal.ca

Funding Information
This work was funded by the Canadian Thoracic Society (CTS) and the Canadian Lung Association (grant-in-aid 2008-2009), and the Atlantic Canada Opportunities Agency Atlantic Innovation Fund 191970, Natural Science and Engineering Research Council Strategic Project Grant 336342. D. Leary gratefully acknowledges support from the Canadian Thoracic Society Studentship. S Svenningsen gratefully acknowledges the support of the National Science and Engineering Research Council CGS-M Scholarship and G. Parraga acknowledges support of a Canadian Institutes of Health Research New Investigator Award.

Received: 2 November 2015; Revised: 14 March 2016; Accepted: 17 March 2016

doi: 10.14814/phy2.12761

Physiol Rep, 4 (7), 2016, e12761, doi: 10.14814/phy2.12761

Abstract

In patients with asthma, magnetic resonance imaging (MRI) provides direct measurements of regional ventilation heterogeneity, the etiology of which is not well-understood, nor is the relationship of ventilation abnormalities with lung mechanics. In addition, respiratory resistance and reactance are often abnormal in asthmatics and the frequency dependence of respiratory resistance is thought to reflect ventilation heterogeneity. We acquired MRI ventilation defect maps, forced expiratory volume in one-second (FEV_1), and airways resistance (Raw) measurements, and used a computational airway model to explore the relationship of ventilation defect percent (VDP) with simulated measurements of respiratory system resistance (R_{rs}) and reactance (X_{rs}). MRI ventilation defect maps were experimentally acquired in 25 asthmatics before, during, and after methacholine challenge and these were nonrigidly coregistered to the airway tree model. Using the model coregistered to ventilation defect maps, we narrowed proximal (9th) and distal (14th) generation airways that were spatially related to the MRI ventilation defects. The relationships for VDP with Raw measured using plethysmography ($r = 0.79$), and model predictions of $R_{rs>14}$ ($r = 0.91$, $P < 0.0001$) and $R_{rs>9}$ ($r = 0.88$, $P < 0.0001$) were significantly stronger ($P = 0.005$; $P = 0.03$, respectively) than with FEV_1 ($r = -0.68$, $P = 0.0001$). The slopes for the relationship of VDP with simulated lung mechanics measurements were different ($P < 0.0001$); among these, the slope for the VDP-$X_{rs0.2}$ relationship was largest, suggesting that VDP was dominated by peripheral airway heterogeneity in these patients. In conclusion, as a first step toward understanding potential links between lung mechanics and ventilation defects, impedance predictions were made using a computational airway tree model with simulated constriction of airways related to ventilation defects measured in mild-moderate asthmatics.

Introduction

Pulmonary imaging using inhaled gas magnetic resonance imaging (MRI) has previously revealed spatially and temporally persistent ventilation defects in chronic obstructive pulmonary disease (COPD) and asthma (de Lange et al. 1999, 2007; Altes et al. 2001; Samee et al. 2003; Parraga et al. 2007). While ventilation MRI is typically acquired in breath-hold, ventilation defects may reflect the ventilation heterogeneity previously estimated using multibreath gas washout (Verbanck et al. 2003; Downie et al. 2007) and positron emission tomography (PET) imaging (Venegas and Musch 2005; Venegas et al. 2005) typically measured using tidal breathing techniques. The size and extent of MRI ventilation defects was previously evaluated in relation to the forced expiratory volume in 1 s (FEV_1) and showed modest correlations in asthma (de Lange et al. 2006) and COPD (Kirby et al. 2010, 2011). In addition, previous work (Costella et al. 2012) also showed weak-to-no relationships for ^{3}He MRI ventilation defect percent (VDP) and FEV_1. Recently, we explored the relationship of MRI ventilation defects and abnormally remodeled airways in asthmatics with and without ventilation defects (Svenningsen et al. 2014), and observed that asthmatics with ventilation defects reported significantly greater inflammation, airways resistance, airflow limitation, and hyper-responsiveness than asthmatics without defects. However, there are still many unanswered questions and some controversy about the role that biomechanical lung abnormalities may play in the temporally and spatially persistent ventilation abnormalities that are visibly and quantitatively obvious in asthmatics.

Pulmonary biomechanics can be estimated using the forced oscillation technique (FOT). Previous FOT studies showed that respiratory system resistance (R_{rs}) and reactance (X_{rs}) were sensitive to heterogeneous airway narrowing (Lutchen and Gillis 1997; Kaczka et al. 1999) and that X_{rs} was particularly sensitive to distal or peripheral airway narrowing (Kaczka et al. 1999). Modeling studies also showed that PET-derived ventilation defects were correlated with respiratory system resistance measured at 0.15 Hz (Tgavalekos et al. 2005, 2007). By simulating bronchoconstriction in an asymmetric branching airway tree model, the relationship of ventilation defects with predictions of R_{rs} and X_{rs} at 6 Hz (Leary et al. 2014) were also shown. In other modeling studies, the distribution of narrowed airways responsible for generating ventilation defects was evaluated as was the relationship of ventilation defects with different frequency-dependent patterns of impedance (Tgavalekos et al. 2005; Campana et al. 2009; Kaczka et al. 2011). The relationship of ventilation defects with respiratory impedance is not well understood; while the frequency dependence of R_{rs} (typically R_{rs} at 5 Hz minus R_{rs} at 20 Hz) and X_{rs} are sensitive to peripheral airway heterogeneity (Lutchen and Gillis 1997; Kaczka et al. 1999), their relative sensitivities, and the physiological relevance of this have not been determined.

To better understand the relationship of respiratory system mechanics and MRI ventilation defects, we coregistered MRI ventilation maps with a computational multibranch airway tree and simulated respiratory measurements after closing airways close to ventilation abnormalities. We explored the relationship of ventilation defects with R_{rs} and the frequency dependence of R_{rs} and X_{rs} as well as experimentally measured FEV_1 and airways resistance (Raw). We hypothesized that lung impedance predictions could be simulated using a model that incorporated ventilation defects measured in asthma patients to help better understand these relationships.

Methods

Study design and subjects

We adapted a three-dimensional airway tree consisting of 64,895 airways (M. Tawhai, U. Auckland), with 32,447 terminal airways (dimension distributions shown in Table 1), to generate an airway tree computational model. A full description of the model was previously provided (Tawhai et al. 2004); briefly, the airway tree was derived from a volume rendered lung X-ray computed tomography (CT) acquired in a patient including the eighth-generation airways with the remaining generations constructed using a volume filling algorithm (Tawhai et al. 2009).

As previously described (Costella et al. 2012), participants between 18 and 60 years of age with diagnosis of asthma and FEV_1 ≥60%, provided written informed consent to a protocol approved by a local research ethics board. During a single two-hour visit, MRI and spirometry were performed at baseline, post-methacholine (at the provocative concentration resulting in a 20% decrease in FEV_1 (PC_{20}) or the final dose) and 25 min after administration of 200 mg salbutamol through a pressurized metered dose inhaler (pMDI) and Aero Chamber Plus valve holding chamber (Trudell Medical International, London, Canada). Spirometry was performed using an ndd EasyOne spirometer (ndd Medizintechnik AG, Zurich, Switzerland). Plethysmography was performed 10 min prior to methacholine challenge using a MedGraphics Elite Series unit (MedGraphics, St. Paul, MN). Methacholine challenge was performed in the seated position according to ATS guidelines (Crapo et al. 2000) using an AeroEclipse II Breath Actuated Nebulizer (Trudell Medical International) until PC_{20} was achieved or a maximum dose of 16.0 mg/mL was administered.

Table 1. Distribution of airway branches and diameters.

Generation *n*	Branches *n*	Terminal Branches *n*	d_{mean} (mm)	d_{max} (mm)	d_{min} (mm)	d_{std} (mm)
1	1	0	14.12	14.12	14.12	0.00
2	2	0	11.13	12.07	10.20	1.32
3	4	0	9.17	10.00	8.00	0.85
4	8	0	6.30	8.00	4.40	1.08
5	16	0	4.62	7.00	3.30	1.22
6	32	0	3.28	6.20	2.69	0.77
7	64	0	2.75	6.00	1.81	0.70
8	128	0	2.27	5.40	1.29	0.54
9	256	2	1.85	3.90	0.79	0.42
10	508	7	1.51	2.90	0.59	0.40
11	1002	56	1.23	2.59	0.50	0.37
12	1892	206	1.01	2.38	0.48	0.32
13	3372	685	0.85	2.23	0.47	0.27
14	5374	1722	0.74	2.01	0.46	0.23
15	7304	2947	0.67	1.85	0.44	0.19
16	8714	4265	0.63	1.70	0.40	0.16
17	8898	4965	0.60	1.57	0.37	0.14
18	7866	4646	0.58	1.39	0.35	0.12
19	6440	4059	0.57	1.24	0.33	0.11
20	4762	3047	0.56	1.09	0.27	0.09
21	3430	2252	0.54	0.96	0.28	0.08
22	2356	1690	0.53	0.85	0.27	0.07
23	1332	992	0.50	0.75	0.34	0.06
24	680	508	0.48	0.71	0.29	0.06
25	344	290	0.43	0.64	0.29	0.07
26	108	108	0.38	0.57	0.24	0.07

d_{mean}, mean airway diameter; d_{max}, maximum airway diameter; d_{min}, minimum airway diameter; d_{std}, standard deviation of airway diameter.

Image acquisition

Anatomical proton (^{1}H) and hyperpolarized ^{3}He MR images were acquired using a 3 Tesla Discovery MR750 system (General Electric Health Care; Milwaukee, WI), as previously described. Subjects (Parraga et al. 2007) were instructed to inhale a fixed 1 L gas mixture (N_2 for ^{1}H MRI and a ^{3}He/N_2 for ^{3}He MRI) from functional residual capacity (FRC), and coronal images were acquired under breath-hold conditions. It is important to note that as previously described, (Costella et al. 2012) the same volume of inhaled gas was used, regardless of FRC or TLC (Table 2). While the signal-to-noise ratio (SNR) was preserved (because we were not in the SNR-limited range), the lung volume relative to TLC for image acquisition was slightly different for each patient. Scans at all time points were performed in the supine position and completed within five minutes of patient positioning in the scanner. Conventional ^{1}H MRI was performed before ^{3}He MRI using the whole-body radiofrequency coil and a fast gradient-recalled echo method (total data acquisition time = 12 sec; TR/TE/flip-angle = 4.3 msec/1.0 msec/30°; FOV=40 × 40 cm; matrix=128 × 80 (zero-padded to 128 × 128); partial echo percent = 62.5%; BW = 62.50 kHz; one excitation; 14 sections; section thickness, 15 mm; zero gap), as previously described.(Parraga et al. 2007) Hyperpolarized ^{3}He MRI was enabled using a rigid linear bird-cage transmit/receive chest coil (RAPID Biomedical GmbH, Wuerzburg, Germany) and ^{3}He gas was polarized to 30–40% using a commercial spin-exchange polarizer system (Polarean Inc, Durham, NC). ^{3}He coronal static ventilation images were acquired using a fast gradient-recalled echo method with partial echo (total data acquisition time = 10 sec; TR/TE/flip-angle = 3.8 msec/1.0 msec/7°; FOV = 40 × 40 cm; matrix = 128 × 80 (zero-padded to 128 × 128); partial echo percent = 62.5%; BW = 62.50 kHz; one excitation; 14 sections; section thickness, 15 mm; zero gap), as previously described (Parraga et al. 2007).

Image analysis

^{3}He MRI semiautomated segmentation was performed using an algorithm implemented in MATLAB (The Math-

Table 2. Baseline demographic characteristics and pulmonary function measurements.

Parameter (±SD)	Asthmatics (n = 25)
Age years	35 (11)
Male/Female	11/14
BMI kg/m^2	26 (5)
$FEV_{1\%pred}$	84 (15)
FVC $\%_{pred}$	93 (11)
FEV_1/FVC %	74 (11)
IC $\%_{pred}$	111 (15)
FRC $\%_{pred}$	92 (15)
RV $\%_{pred}$	113 (25)
TLC $\%_{pred}$	101 (9)
Raw $\%_{pred}$	126 (69)*
Gaw $\%_{pred}$	63 (38)*
PC_{20} mg/mL	6 (23)

SD, Standard Deviation; BMI, Body Mass Index; FEV_1, Forced Expiratory Volume in 1s; $\%_{pred}$, Percent Predicted; FVC, Forced Vital Capacity; IC, Inspiratory Capacity; FRC, Functional Residual Capacity; RV, Residual Volume; TLC, Total Lung Capacity; Raw, Airway Resistance; Gaw, Airway Conductance; PC_{20}, provocative concentration of methacholine sufficient to induce a 20% decrease in FEV.
*n = 24.

works Inc., Natick, MA), as previously described (Kirby et al. 2012). Briefly, and as shown in Figure 1, ^{3}He MRI static ventilation images were segmented using a K-means approach that classified voxel intensity values into five clusters ranging from signal void (cluster 1, C1 or ventilation defect volume [VDV]) and hypointense (or partial volume) to hyperintense signal (C5). The delineation of the ventilation defect boundaries was performed using a seeded region-growing algorithm that segmented the ^{1}H MRI thoracic cavity, as previously described (Kirby et al. 2012). This approach was previously validated using ventilation images in patients with asthma, cystic fibrosis, and COPD, and was based on a previous definition of ventilation defect volume as cluster 1 based on an expert visual interpretation of a series of images. Based on this previous information and numerous previous studies (Costella et al. 2012; Kirby et al. 2012; Svenningsen et al. 2014; Pike et al. 2015), we used this definition in this study.

Coregistration of MRI ventilation maps to airway tree

We used rigid and nonrigid registration algorithms in MATLAB to coregister the MRI ventilation cluster map with the airway tree model. Briefly, the lung model was first resampled anterior-to posterior into the same number of 15 mm slices as the coronal MRI datasets. A transformation matrix was generated so that each of the MRI coronal slices was rigidly coregistered to the mesh in the x, y, and z direction. Next, eight to 10 fiducial landmarks were manually located along the outer lung boundaries for each slice and using these fiducials, individual slices were rigidly coregistered to the mesh. This was performed for all datasets. It is also important to note that the rather coarse spatial resolution of the MR coronal slices was 3.13 mm_x × 3.13 mm_y × 15 mm_z and this places a conservative limit on registration accuracy. We note that we have routinely coregistered CT airway trees from individual patients to the MRI functional datasets in this manner (Pike et al. 2015) with fiducial localization error of 3–6 mm in the x and y plane and Dice similarity coefficients similar to what was achieved here (mean DSC = 83 ± 3%). In Figure 2, we show the coregistration

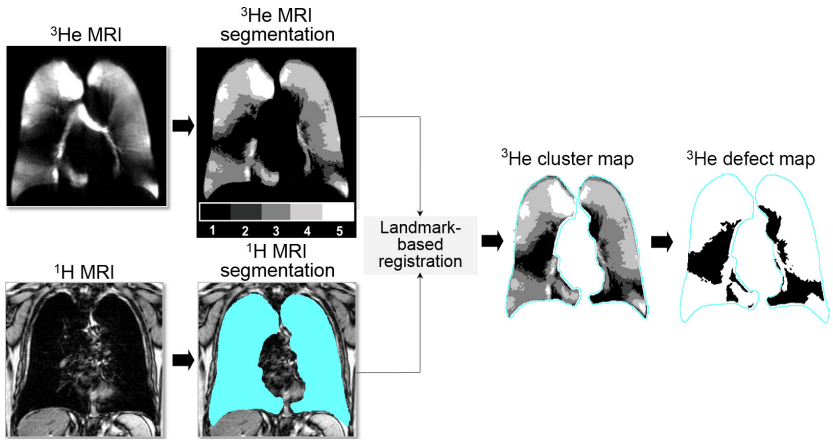

Figure 1. Pipeline for segmentation of ^{3}He MRI ventilation defects. Raw image data from ^{3}He MRI and conventional proton MRI are coregistered and a k-means cluster algorithm was used to segment ventilation defects (shown as Cluster 1).

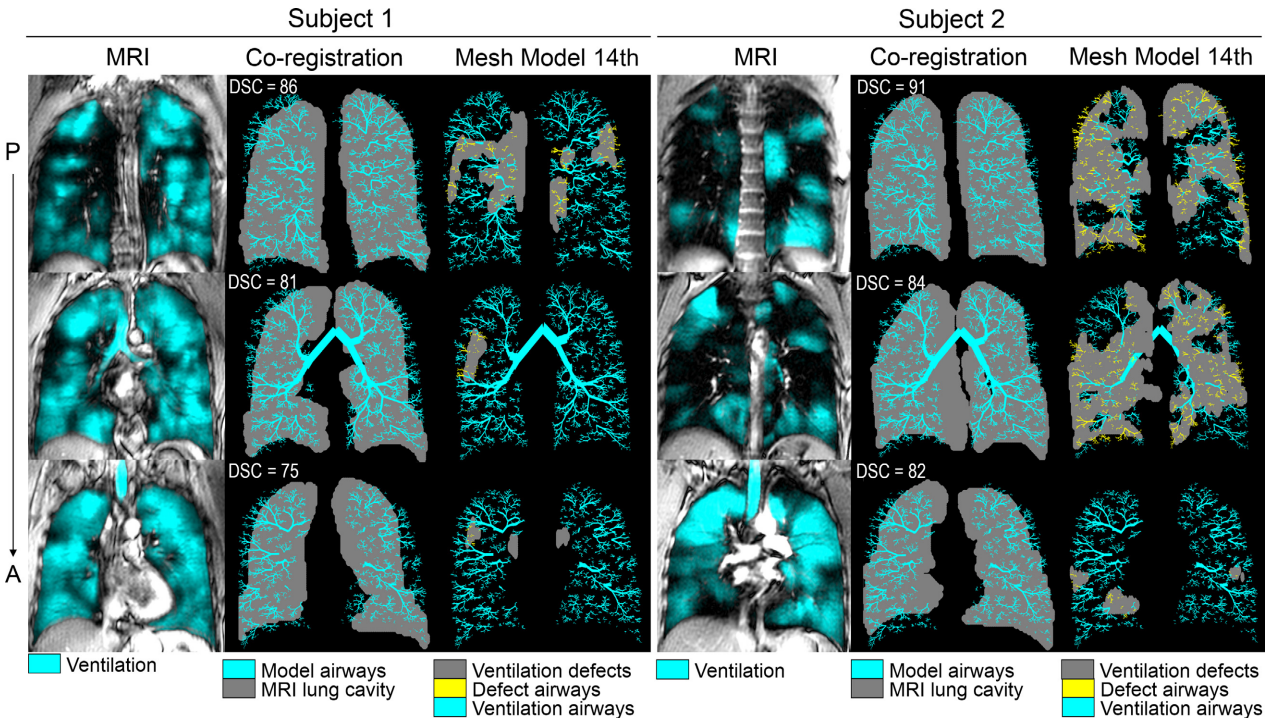

Figure 2. Coregistration of MRI and airway mesh model for three center slices in two representative asthmatics. For Subject 1 and 2, left panels show center, and 2 slices anterior (A) and posterior (P) to center coronal slice MRI; middle panels show corresponding model-to-MRI lung cavity coregistration; right panels show coregistration of model-to-ventilation defects coregistration with 14th generation airways proximal to ventilation defects closed in yellow. Slice-specific Dice similarity coefficients (DSC) reflect registration accuracy for each of the three slices coregistered to the airway model for each of Subject 1 and 2.

results for three slices for each of the two subjects. The DSC ranged from 86 to 75% for Subject 1 and 91–82% for Subject 2, and this provides good evidence of coregistration accuracy. Figure 2 also shows the spatial relationship of 14th generation airways that were narrowed proximal to ventilation defects in these subjects.

Impedance Predictions

Airways within ventilation defects (>10 voxels in the x or y direction (or 3 cm)) were narrowed to 10% of initial diameter as this effectively increased resistance by a factor of 10^4 according to Poiseuille's law and avoided diameters of zero in the simulations (Tgavalekos et al. 2005). We occluded airways located within ventilation defects and within two voxels of their boundary at two different airway generations (9th or 14th generations) as shown in Figure 2 for two representative subjects, with airways proximal to ventilation defects shown in yellow and the ventilation abnormalities shown in gray. The rationale for choosing both 9th and 14th generation airways was based on previous work (Tgavalekos et al. 2005) that endeavored to explore simulations stemming from the medium and small airways. It is important to note that for trained image observers, it is quite straightforward to identify the specific airways leading to ventilation defects including the relatively large continuous spatial clusters >10 voxels we evaluated here. It is also worth pointing out that many ventilation defects were segmental and subsegmental defects as shown in Figures 2 and 3, and in these cases, the airway ventilation defect spatial concordance is also anatomically obvious.

Lung model impedance predictions were generated as previously described (Bhatawadekar et al. 2015) where the initial lung volume was reduced from TLC to FRC by reducing the airway diameters and lengths to 80%, achieving a volume ratio of 0.5. Flow was described by Womersley (Kaczka et al. 2007) where the complex impedance of each nonterminal airway branch was calculated as

$$Z_a(f) = \frac{j2f\rho_{air}l_a}{{r_a}^2}\left[1 - \frac{2J_1(\alpha_a\sqrt{-j})}{\alpha_a\sqrt{-j}J_0(\alpha_a\sqrt{-j})}\right]^{-1} \quad (1)$$

where r_a is the radius and l_a is the length of the airway, f is the oscillation frequency in Hz, ρ_{air} is the density of air (1.16 kg/m^3), J_0 and J_1 are the complex Bessel functions of order 0 and 1, respectively, j, the unit imaginary num-

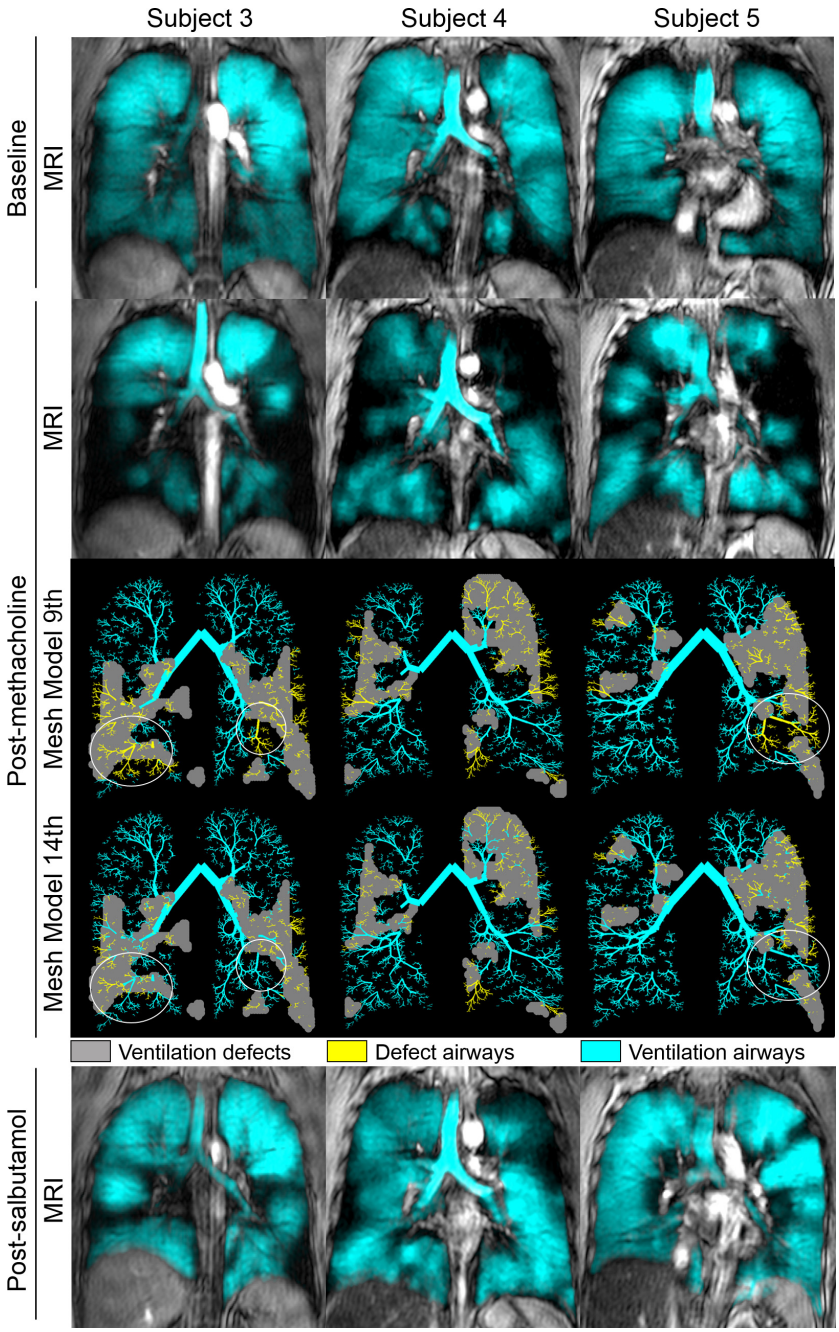

Figure 3. MRI and model-to-MRI coregistration for three asthmatics showing colocalization of airway tree and ventilation defects post-methacholine. Center coronal slice MRI ventilation in blue coregistered to anatomical MRI in gray scale at baseline, post-methacholine and post-salbutamol. For each subject, the corresponding post-methacholine mesh models with closure of airways from 9th (Row 3 across) or 14th generation (Row 4 across) are shown. For the mesh model, gray reflects an MRI ventilation defect, yellow segments are specific to mesh model airways located within a ventilation defect and cyan segments airways were mesh model airways that did NOT lead to ventilation defects. White circles show differences reflected by closure of either the 9th (row 3) or 14th (row 4) generation airways in the model. Subject 3: 36-year-old female; baseline/post-methacholine/post-salbutamol FEV_1 = 66/45/71%$_{pred,}$ VDP = 9/50/10%, $R_{rs>9}$ = 2.97/4.64/3.12 $cmH_2O.s.L^{-1}$, $R_{rs>14}$ = 2.71/3.54/2.78 $cmH_2O.s.L^{-1}$, $X_{rs>9}$ = −2.20/−3.93/−2.16 $cmH_2O.s.L^{-1}$ and $X_{rs>14}$=−1.64/−2.68/−1.49 $cmH_2O.s.L^{-1}$. Subject 4: 42 year-old male; baseline/post-methacholine/post-salbutamol FEV_1 = 72/50/77%$_{pred,}$ VDP = 8/25/9%, $R_{rs>9}$ = 2.71/4.08/3.04 $cmH_2O.s.L^{-1}$, $R_{rs>14}$ = 2.67/3.21/2.76 $cmH_2O.s.L^{-1}$, $X_{rs>9}$ = −1.63/−4.28/−2.35 $cmH_2O.s.L^{-1}$ and $X_{rs>14}$ = −1.43/−2.51/−1.62 $cmH_2O.s.L^{-1}$. Subject 5: 46-year-old male; baseline/post-methacholine/post-salbutamol FEV_1 = 60/43/62%$_{pred,}$ VDP = 3/21/3%, $R_{rs>9}$ = 2.72/3.94/2.73 $cmH_2O.s.L^{-1}$, $R_{rs>14}$ = 2.64/3.22/2.63 $cmH_2O.s.L^{-1}$, $X_{rs>9}$ = −1.46/−3.45/−1.37 $cmH_2O.s.L^{-1}$ and $X_{rs>14}$ = −1.21/−2.03/−1.14 $cmH_2O.s.L^{-1}$.

ber, and α_a is the Womersley number of the airway branch given by

$$\alpha_a = r_a\sqrt{\frac{2\Pi\rho_{air}f}{\mu_{air}}} \quad (2)$$

where μ_{air} is the dynamic viscosity of humid air at 37°C (1.85×10^{-5} Pa.s). Lung compliance was distributed evenly at terminal airways as each served as an alveolar compartment accounting for parenchymal stretch, surface tension, and gas compression (Tgavalekos et al. 2003). We recognize that this approach neglects the contributions of airway wall compliance and gas compression within airways, but this effect is much smaller than the effect of the alveolar compartment (Mead 1979; Leary et al. 2014). The impedance of each terminal airway was defined as

$$Z_t = Z_a - j\frac{Et}{\omega} \quad (3)$$

where E_t is the elastance of the terminal airway unit. The model lung impedance ($Z_{L,mod}$) was evaluated from series and parallel summations of all airway impedances assuming a lumped element approach, and separated into resistance ($R_{L,mod}$) and reactance ($X_{L,mod}$), and evaluated from 0.2 to 32 Hz.

Upper airway resistance ($R_{central}$) and chest wall resistance (R_{cw}) were assigned values of 0.5 $cmH_2O.s.L^{-1}$ each (Nagels et al. 1980; Barnas et al. 1987, 1989) and these were added to R_{Lmod} to obtain the model respiratory system resistance R_{rs}. Due to the high-frequency dependence of X_{rs}, we also computed elastance which is largely frequency independent in healthy lung. Chest wall elastance (E_{cw} = 10.6 $cmH_2O.s.L^{-1}$) (Barnas et al. 1985) was summed with lung elastance ($E_{rs,mod}$) to obtain the respiratory system elastance (E_{rs}), where E_{rs} was $2.\pi.f.X_{rs}(f)$. We computed E_{rs} for low frequencies only where X_{rs} was dominated by elastic mechanics. The frequency dependence of R_{rs} was evaluated over two ranges: 1) the low-frequency range of 0.2–5 Hz ($R_{rs}0.2–R_{rs}5$) which is normally not accessible by common forced oscillation methods (but where the frequency dependence of R_{rs} is more easily observed), and, 2) the oscillometry frequency range of 5–20 Hz ($R_{rs}5–R_{rs}20$). Finally, the effects of upper airway shunt (Z_{uaw}) were implemented using previously published Z_{uaw} values (Cauberghs and Van de Woestijne 1983) and extrapolated values of shunt resistance and reactance at 0.2 Hz as previously described (Bhatawadekar et al. 2015).

Statistical analysis

Data were tested for normality using the Shapiro–Wilk normality test and nonparametric tests were performed when data were not normal. Univariate relationships were evaluated using linear regressions (r^2), Pearson correlations (r), and Spearman correlations (ρ) when the data were not normal generated using GraphPad Prism version 4.00 (GraphPad Software, Inc., San Diego, CA). The Fisher z transformation was used to determine significant differences between r values. Significant differences in the VDP-impedance relationship slopes were determined using analysis of covariance (ANCOVA). Holm–Bonferonni corrections were used for multiple comparisons. All results were considered statistically significant when the probability of making a Type 1 error was less than 5% ($P < 0.05$).

Results

Subjects

Table 2 provides subject demographic and pulmonary function measurements for 25 mild-moderate participants with asthma (mean age 35 ± 11 years), moderately abnormal FEV_1/FVC and airways resistance (Raw = 126 ± 69%$_{pred}$). Figure 3 shows ventilation images (pre and post-methacholine and post-salbutamol) and model-to-MRI coregistration results (post-methacholine) for three asthmatics. For all three subjects, methacholine induced a larger size and greater number of ventilation defects that partially resolved post-salbutamol. The coregistered model-to-MRI results show the spatial localization of the 14th or 9th generation airways closed within ventilation defects and used to generate the simulated impedance measurements.

Model and experimental measurements

In Figure 4, the frequency-dependent R_{rs} and X_{rs} predictions at baseline, post-methacholine, and post-salbutamol are provided. Table 3 shows measurements acquired and model predictions related to these three conditions. FEV_1, VDP, and model predictions of R_{rs} and X_{rs} at 5 Hz were significantly different post-methacholine and post-salbutamol. Underscoring these significant differences, in Table 4, the fractional changes (baseline – post-methacholine and post-methacholine – post-salbutamol) are shown for $R_{rs>14}$ at different frequencies and frequency bands.

Relationships for experimental measurements and model predictions

Table 5 shows correlation coefficients for FEV_1%, Raw%, and model-derived R_{rs} and X_{rs} at 5 Hz with VDP. There were moderate correlations for VDP with FEV_1% and Raw % and significantly stronger correlations with R_{rs} and X_{rs}. Some of these relationships are also shown in Figure 3 and

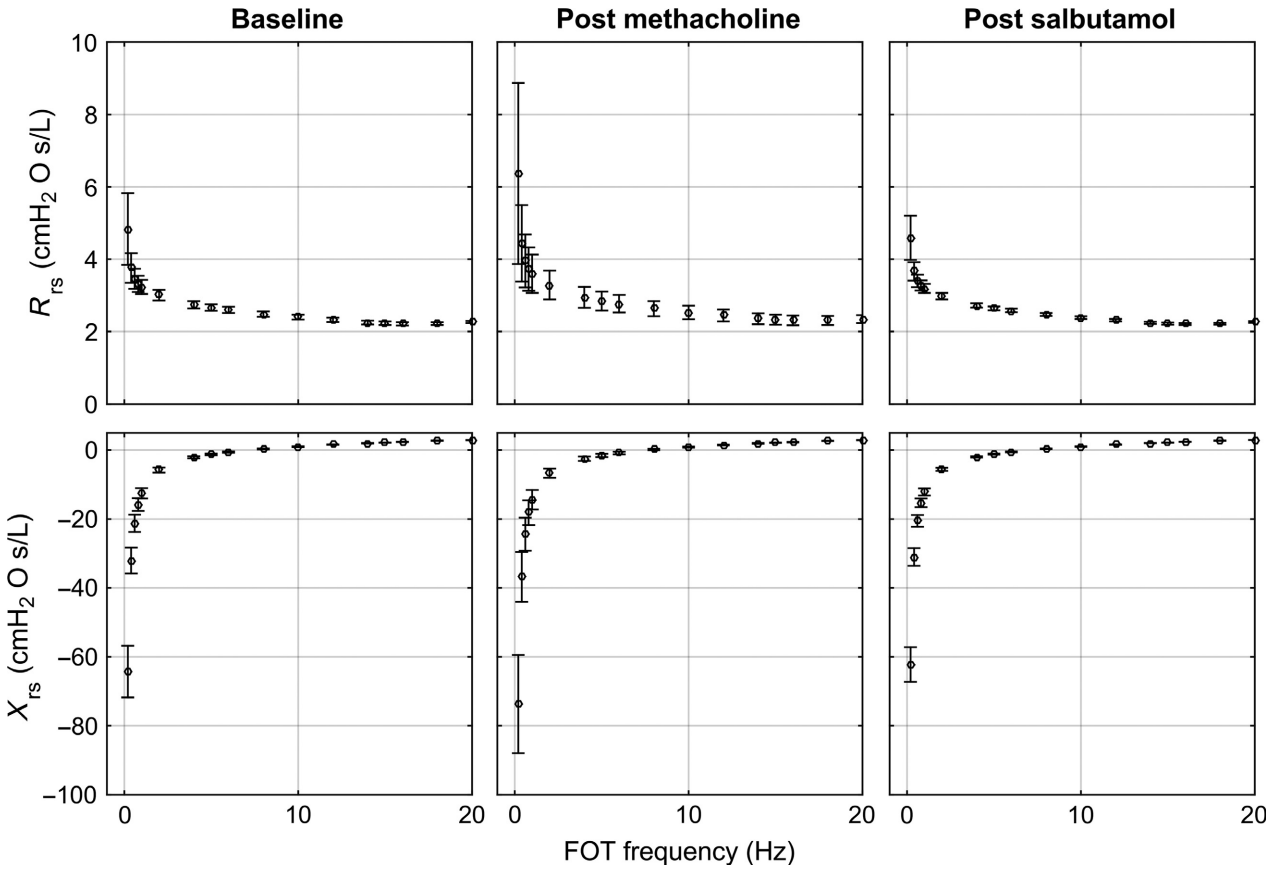

Figure 4. R_{rs} and X_{rs} versus frequency at baseline, post-methacholine, and post-salbutamol. Each point represents the mean value of the predictions for the 25 patients and the error bars represents the standard deviation of the distribution.

Table 3. Baseline, post-methacholine and post-salbutamol FEV_1, VDP and model predictions.

Parameter (±SD)	Baseline (n = 25)	Post-methacholine (n = 25)	Post-Salbutamol (n = 25)	P-value*
Experimental				
$FEV_{1\%pred}$	84 (15)	64 (15)	87 (15)	<0.0001
VDP %	4 (4)	11 (10)	4 (2)	0.0002
Model				
$R_{rs>9}$ $cmH_2O.s.L^{-1}$	1.99 (0.26)	2.33 (0.67)	1.92 (0.11)	0.003
$R_{rs>14}$ $cmH_2O.s.L^{-1}$	1.85 (0.09)	2.00 (0.24)	1.84 (0.06)	0.002
$X_{rs>9}$ $cmH_2O.s.L^{-1}$	−1.16 (0.34)	−1.54 (0.73)	−1.07 (0.18)	0.0008
$X_{rs>14}$ $cmH_2O.s.L^{-1}$	−0.95 (0.13)	−1.14 (0.27)	−0.92 (0.09)	<0.0001

SD, Standard Deviation; FEV_1, Forced Expiratory Volume in 1s; $\%_{pred}$, Percent Predicted; VDP, Ventilation Defect Percent; R_{rs}, lung resistance; $R_{rs>9}$, model prediction of R_{rs} when airways were closed distal to the 9th generation; $R_{rs>14}$, model prediction of R_{rs} when airways were closed distal to the 14th generation; X_{rs}, lung reactance; $X_{rs>9}$, model prediction of X_{rs} when airways were closed distal to the 9th generation; $X_{rs>14}$, model prediction of X_{rs} when airways were closed distal to the 14th generation.
*Repeated measures analysis of variance.

4. Figure 5 shows the relationship of Raw% measured before methacholine provocation with model predictions of R_{rs} when airways were closed from the 9th (r = 0.71, P < 0.0001) and 14th generation (r = 0.71, P = 0.0003).

As shown in Figure 6, R_{rs} was increased and X_{rs} at 5 Hz was diminished in relation to increasing (or worse) VDP. Figure 6A and B show impedance predictions at 5 Hz and the strong correlations between R_{rs} and VDP for 9th gener-

Table 4. Fractional changes in VDP, FEV_1 and model predictions post-methacholine (relative to baseline) and post-salbutamol (relative to post-methacholine).

Parameter (±SD)	Post- methacholine/ Baseline (n = 25)	Post-Salbutamol/ Post-methacholine (n = 25)
Experimental		
$FEV_{1\%pred}$	0.76 (0.07)	1.37 (0.17)
VDP (%)	2.96 (1.50)	0.38 (0.20)
Model		
$R_{rs0.2}$	1.31 (0.19)	0.77 (0.26)
R_{rs5}	1.07 (0.06)	0.94 (0.07)
R_{rs20}	1.03 (0.33)	0.97 (0.04)
$R_{rs0.2\text{-}5}$	1.25 (0.16)	0.07 (0.23)
$R_{rs5\text{-}20}$	1.56 (0.22)	0.45 (0.34)
$X_{rs0.2}$	1.14 (0.08)	0.86 (0.11)
X_{rs5}	1.26 (0.10)	0.78 (0.16)
X_{rs20}	0.99 (0.01)	1.02 (0.01)

SD, Standard Deviation; FEV_1, Forced Expiratory Volume in 1s; $\%_{pred}$, Percent Predicted; VDP, Ventilation Defect Percent; R_{rs}, lung resistance; $R_{L0.2}$, model prediction of R_{rs} measured at 0.2 Hz, R_{rs5}, model prediction of R_{rs} measured at 5 Hz, R_{L20}, model prediction of R_{rs} measured at 20 Hz, $R_{rs0.2\text{-}5}$, difference in model prediction of R_{rs} measured at 0.2–5 Hz, $R_{rs5\text{-}20}$, model prediction of R_{rs} measured at 20–5 Hz, $X_{L0.2}$, model prediction of X_{rs} measured at 0.2 Hz, X_{rs5}, model prediction of X_{rs} measured at 5 Hz, and X_{rs20}, model prediction of X_{rs} measured at 20 Hz.

Table 5. Relationships for FEV_1, Raw, and model-derived measurements at 5 Hz with Raw and VDP.

	Raw $\%_{pred}$ (n = 24) r (p)	VDP % (n = 75) r (p)
Experimental		
$FEV_{1\%pred}$	−0.74 (<0.0001)	−0.68 (<0.0001)
Raw $\%_{pred}$	–	0.79 (<0.0001)*
Model		
$R_{rs>9}$	0.71 (<0.0001)	0.88 (<0.0001)
$R_{rs>14}$	0.71 (<0.0001)	0.91 (<0.0001)
$X_{rs>9}$	–	−0.88 (<0.0001)
$X_{rs>14}$	–	−0.94 (<0.0001)

Raw, Airway Resistance; VDP, Ventilation Defect Percent; FEV_1, Forced Expiratory Volume in 1s; $\%_{pred}$, Percent Predicted; R_{rs}, lung resistance; $R_{rs>9}$, model prediction of R_{rs} when airways were closed distal to the 9th generation; $R_{rs>14}$, model prediction of R_{rs} when airways were closed distal to the 14th generation; X_{rs}, lung reactance; $X_{rs>9}$, model prediction of X_{rs} when airways were closed distal to the 9th generation; $X_{rs>14}$, model prediction of X_{rs} when airways were closed distal to the 14th generation; r = Pearson r correlation coefficient.
*n = 24.

ation (r = 0.88, $P < 0.0001$) and 14th generation (r = 0.91, $P < 0.0001$) airway closures, respectively. Figure 6C and D also show strong correlations between X_{rs} at 5 Hz and VDP for 9th (r = −0.88, $P < 0.0001$) and 14th generation (r = −0.94, $P < 0.0001$) airway closures, respectively. The relationship between $R_{rs>14}$ and VDP was significantly stronger than with FEV_1 (z = 2.79, P = 0.005), but not with Raw (z = 1.86, P = 0.06). $R_{rs>9}$ was more strongly correlated with VDP than with FEV_1 (z = 2.24, P = 0.03), but not Raw (z = 1.31, P = 0.19). The correlation between $X_{rs>14}$ and VDP was significantly stronger than the correlation between $X_{rs>9}$ and VDP (z = 2.40, P = 0.02), whereas the relationships for $R_{rs>14}$ and $R_{rs>9}$ with VDP were not significantly different (z = 0.94, P = 0.34).

As shown in Figure 7, model predictions of R_{rs} and X_{rs} were strongly linearly correlated with VDP (at 5 Hz, R_{rs}, r = 0.94, $P < 0.0001$; $X_{rs,}$ r = 0.92, $P < 0.0001$), and these relationships weakened at greater frequencies. In Figure 8, the relationships for impedance measures with VDP are shown at specific frequencies, and the magnitude of these slopes are provided in Table 6. The slope that described the relationship for $R_{rs0.2}$ and VDP was significantly greater than for the R_{rs5}–VDP relationship ($P < 0.001$) and also significantly greater than the R_{rs20} –VDP relationship ($P < 0.001$). In a similar manner, the slope for the $X_{rs0.2}$–VDP relationship was more negative than the X_{rs5}–VDP relationship ($P < 0.001$). At all frequencies, the relationships between VDP and X_{rs} were stronger than those between VDP and R_{rs}. For example, in the typical FOT range at 5 Hz, the X_{rs5}–VDP relationship was stronger than R_{rs5}–VDP ($P < 0.001$) and the $R_{rs5\text{-}20}$ –VDP ($P < 0.001$) relationships. The slopes for the relationship of E_{rs} with VDP are also apparently greater than the 5 Hz X_{rs}–VDP relationship, but the larger slope is due to the change in units for E_{rs} to $cmH_2O.L^{-1}$ and not due to a stronger correlation.

Discussion

We used ventilation defect maps acquired in asthmatics to constrain airway closure in a computational airway tree model and simulated measurements of airways resistance to investigate the influence of airway narrowing related to ventilation defects with predictions of lung biomechanical measurements and observed: (1) MRI ventilation measurements in 25 asthmatics acquired before, during, and after methacholine challenge could be used to close specific airways and drive simulations of lung biomechanical behavior, (2) model predictions showed greater mean R_{rs} and lower X_{rs} when specific airways were narrowed based on their proximity to MRI ventilation defects measured post-methacholine, and (3) when ventilation defects were

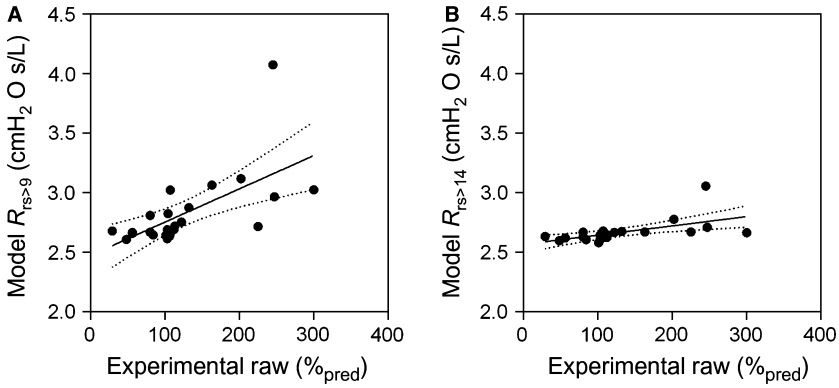

Figure 5. Relationship for Raw $\%_{pred}$ with model predictions of R_{rs} ($cmH_2O.s.L^{-1}$) at 5 Hz. Experimentally measured Raw $\%_{pred}$ using plethysmography at baseline compared with model predictions of R_{rs} based on airways distal to ventilation defects maximally closed at the A) 9th generation ($r = 0.71$, $r^2 = 0.39$, $P < 0.0001$, $y = 0.003x + 2.47$) and B) 14th ($r = 0.71$, $r^2 = 0.34$, $P < 0.0001$, $y = 0.0008x + 2.57$) generation.

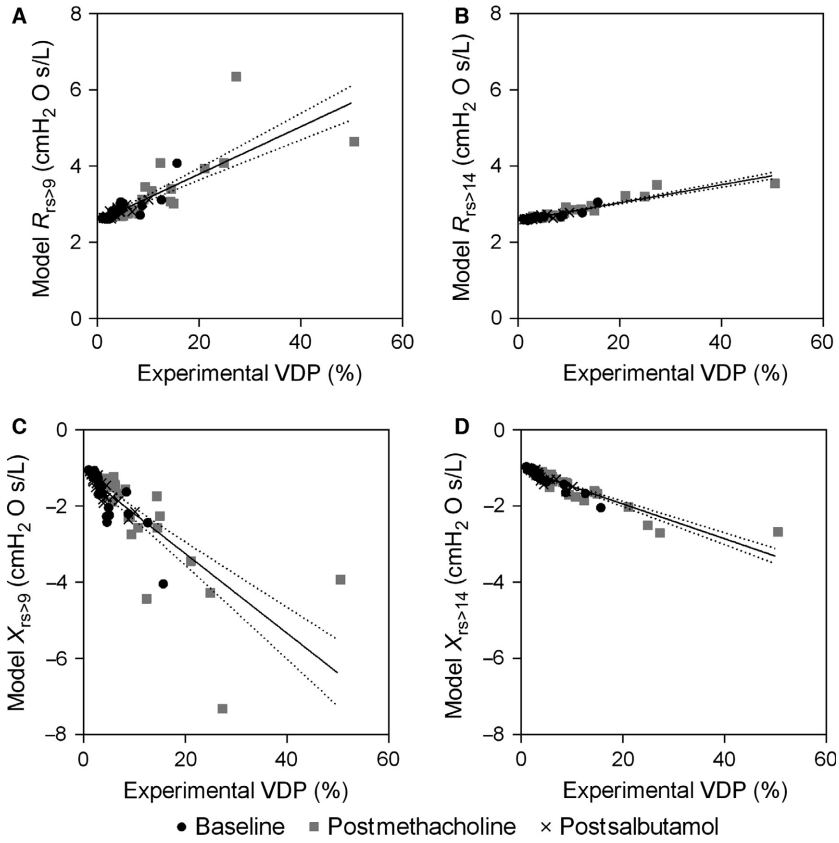

Figure 6. Relationship for ^{3}He MRI VDP with model predictions of R_{rs} and X_{rs} at 5 Hz. There were significant relationships for VDP and model predictions of R_{rs} related to simulations of airways distal to ventilation defects maximally closed at the A) 9th ($r = 0.88$, $r^2 = 0.67$, $P < 0.0001$, $y = 0.06x + 2.54$) and B) 14th ($r = 0.91$, $r^2 = 0.89$, $P < 0.0001$, $y = 0.02x + 2.56$) generation, and model predictions of X_{rs} at the C) 9th ($r = -0.88$, $r^2 = 0.60$, $P < 0.0001$, $y = -0.01x - 1.16$) and D) 14th ($r = -0.94$, $r^2 = 0.85$, $P < 0.0001$, $y = -0.05x - 1.03$) generation.

used to regionally constrain airway closure, the relationship between model predictions of X_{rs} and VDP was greater when more distal airways (14th vs. the 9th generation) were perturbed.

In asthma patients, ventilation defects increase in number and size during methacholine challenge and respiratory system resistance also increases (Tgavalekos et al. 2007). In a previous study, the relationship between PET-

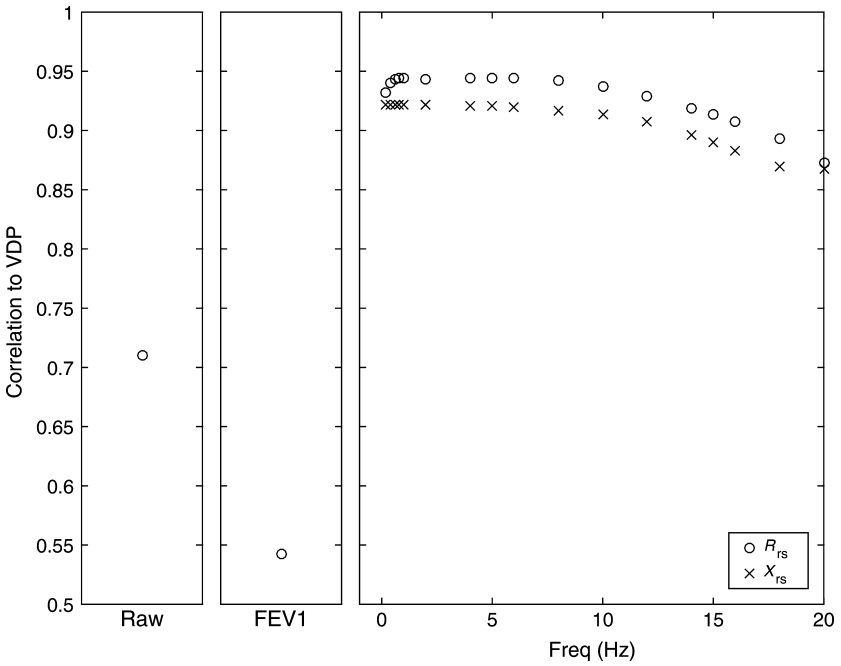

Figure 7. VDP correlations with experimentally measured Raw%$_{pred}$ at baseline, FEV$_1$%$_{pred}$ and model predictions for R_{rs} and X_{rs} over a range of test frequencies.

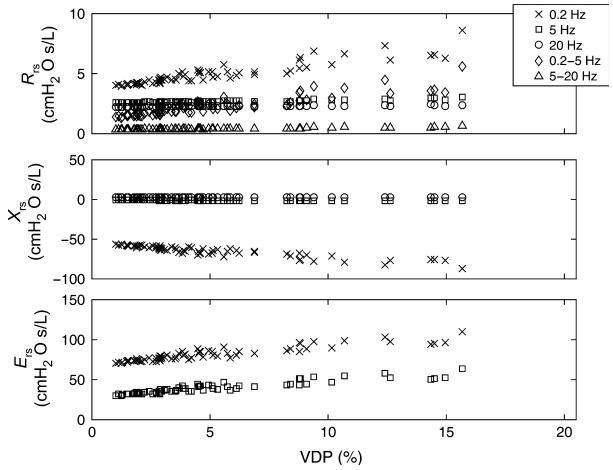

Figure 8. The sensitivity of measurements predicted by the lung model at various frequencies as indicated by the legend. The sensitivity to changes in VDP are indicated by increased slope (slopes for each frequency provided in Table 6). Measurements at lower frequencies showed greater dependence to VDP (i.e., X_{rs} and E_{rs} measured at 0.2 Hz reflected the greatest sensitivity to changes in VDP).

Table 6. Relationships for model predictions with VDP.

Model prediction	Slope
$R_{rs0.2}$	0.223
R_{rs5}	0.024
R_{rs20}	0.009
$R_{rs0.2\text{-}5}$	0.199
$R_{rs5\text{-}20}$	0.015
$X_{rs0.2}$	−1.356
X_{rs5}	−0.046
X_{rs20}	−0.005
$E_{rs0.2}$	1.703
E_{rs5}	1.435

derived ventilation defects and lung impedance was dependent on distal airway closure (Tgavalekos et al. 2005). Similar to this previous work, our model was constrained to physiologically relevant ventilation defects observed in a relatively wide variety of mild-to-moderate asthmatics. While it was not surprising that impedance increased with experimentally derived VDP, we were surprised that in asthma patients, this relationship was linear and statistically greater at the lower frequencies (in the range typically used by oscillometry). We also observed that when ventilation defects are used to regionally constrain airway closure, the relationship between model predictions of X_{rs} and VDP was greater when more distal airways (14th vs. 9th generation) were perturbed. While the physiological meaning of these findings is yet to be determined, as first demonstrated by Otis (Otis et al. 1956) using a single bifurcating airway, resistance and reactance are interdependent. In a homogeneous bifurcat-

ing airway tree, X_{rs} yields information related to the combined effect of the elastic and inertive properties of the lung where elastic effects dominate at low frequencies. In obstructive lung diseases like asthma, low-frequency X_{rs}, and thus E_{rs} can be strongly influenced by small airway narrowing, even, as our model suggested, when there are no changes in intrinsic tissue stiffness. This may reflect derecruitment of parenchyma whereby airway narrowing prevents distal oscillatory flow to the parenchyma diminishing lung elastance indicated by the more negative X_{rs}. Although we observed the X_{rs5}–VDP relationship was stronger in the distal airways, it is difficult to be certain about the physical meaning of this finding. It is important to note that we did not observe different R_{rs5}–VDP correlations for the distal versus proximal airways. Taken together, however, these data suggest that R_{rs5} may be less sensitive than X_{rs5} and E_{rs} to conditions whereby the small airways are narrowed sufficiently to prevent oscillatory flow. Notably, previous work in pigs showed that R_{rs} was sensitive to airway narrowing and X_{rs} was more sensitive to ventilation defects (Dellaca et al. 2009).

The finding that X_{rs5} and E_{rs} predictions were related to VDP warrants further investigation and experimental confirmation in asthmatics. However, at 0.2 Hz, where the slope for the relationship between X_{rs} and VDP was the greatest, experimental confirmation will be challenging. Low-frequency respiratory impedance can be determined using the optimal ventilation waveforms, but this approach is not amenable to clinical use. At the more common FOT frequencies, such as 5 Hz, model predictions of X_{rs} (and therefore E_{rs}) were more sensitive to VDP than the frequency dependence of R_{rs} from 5 to 20 Hz. This sensitivity may arise from the peripheral airway narrowing which leads to alveolar derecruitment. However, the greater sensitivity of X_{rs} at 5 Hz compared to R_{rs} may be explained because resistance measurements at 5 Hz and 20 Hz include a large contribution from mainly unobstructed central airways. Low-frequency X_{rs} and E_{rs} are dominated by the compliant parenchyma, with smaller contributions from the chest wall. This is in contrast to the small contribution of the peripheral airway relative to the upper and central airways to R_{rs}, which may explain why airway narrowing in the periphery had a greater effect on X_{rs} than R_{rs}.

Our study was limited and in that, we did not experimentally acquire oscillometry measurements; therefore, it is difficult to be certain about the physiological meaning of the relationships observed here between ventilation defects and respiratory resistance/reactance. Given the temporal nature of asthma provocation, it will be very difficult logistically to acquire these data experimentally within a methacholine challenge. Nonetheless, this modeling study cannot be considered definitive, but a hypothesis-generating exploration of how an airway tree model can be used and constrained to help better understand resistance and reactance in asthmatics. Our model was limited and in that, we did not account for small degrees of constriction or dilation in the airways throughout the remaining lung volume – namely, the ventilated regions or central airways. This is important because lung regions outside of ventilation defects may be partially inflated or hyperinflated and this would alter R_{rs}. We recognize that in asthmatics, ventilation defects are unlikely due to airway closure at specific generations. A possible future improvement in the model can be undertaken whereby more complex airway lumen sizing techniques at different generations can be used to scale airway diameter. It is also important to emphasize that we did not test how different spatial distributions of ventilation defects or patterns of bronchoconstriction influenced lung impedance. Therefore, we cannot comment on the sensitivity or specificity of impedance predictions to the spatial pattern of ventilation defects. However, despite normal variation in defect size and distribution among the subjects, we observed that experimentally measured Raw and predicted Rrs and Xrs at 5 Hz were strongly correlated with VDP. Also, we did not include upper airway narrowing in these simulations, but this could certainly lead to greater R_{rs} variability, relative to X_{rs}.

Ventilation heterogeneity is a hallmark finding in both asthma and COPD, but the biomechanical mechanisms responsible for ventilation defects in COPD and asthma may differ. In asthma patients, ventilation defects may be due to increased muscle activation acting on a normal parenchymal tethering load and/or mucous plugging (Downie et al. 2007). In COPD, there is the potential for diminished elastic recoil and thickened airway walls (Hogg et al. 2004). Indeed, in severe COPD, ventilation defects are regionally related to both emphysematous bullae and airway abnormalities (Kirby et al. 2014). In summary, we used an airway tree model to generate simulations of R_{rs} and X_{rs} based on ventilation defects in 25 asthmatics. Model predictions of low-frequency X_{rs} and E_{rs} provide a way to explain airway behavior that may result in ventilation defects in asthmatics.

Acknowledgments

The authors thank M. Tawhai for the generous provision of the airway dimension data, S. Blamires for clinical coordination and database management, A. Wheatley for gas contrast dispensing and administration, and T. Szekeres for MRI of research volunteers.

Conflict of Interest

The authors declare they have no conflicts of interest to declare.

References

Altes, T. A., P. L. Powers, J. Knight-Scott, G. Rakes, T. A. Platts-Mills, E. E. de Lange, et al. 2001. Hyperpolarized ^{3}He MR lung ventilation imaging in asthmatics: preliminary findings. J. Magn. Reson. imaging: JMRI 13:378–384.

Barnas, G. M., K. Yoshino, J. Fredberg, Y. Kikuchi, S. H. Loring, and J. Mead. 1985. Total and local impedances of the chest wall up to 10 Hz. J. Appl. Physiol. 68:1409–1414. 1990

Barnas, G. M., K. Yoshino, S. H. Loring, and J. Mead. 1987. Impedance and relative displacements of relaxed chest wall up to 4 Hz. J. Appl. Physiol. 62:71–81.

Barnas, G. M., K. Yoshino, D. Stamenovic, Y. Kikuchi, S. H. Loring, and J. Mead. 1989. Chest wall impedance partitioned into rib cage and diaphragm-abdominal pathways. J. Appl. Physiol. 66:350–359.

Bhatawadekar, S. A., D. Leary, and G. N. Maksym. 2015. Modelling resistance and reactance with heterogeneous airway narrowing in mild to severe asthma. Can. J. Physiol. Pharmacol. 93:207–214.

Campana, L., J. Kenyon, S. Zhalehdoust-Sani, Y. S. Tzeng, Y. Sun, M. Albert, et al. 2009. Probing airway conditions governing ventilation defects in asthma via hyperpolarized MRI image functional modeling. J. Appl. Physiol. 106:1293–1300.

Cauberghs, M., and K. P. Van de Woestijne. 1983. Mechanical properties of the upper airway. J. Appl. Physiol. Respir. Environ. Exerc. Physiol. 55:335–342.

Costella, S., M. Kirby, G. N. Maksym, D. G. McCormack, N. A. Paterson, and G. Parraga. 2012. Regional Pulmonary Response to a Methacholine Challenge using Hyperpolarized ^{3}He Magnetic Resonance Imaging. Respirology 17:1237–1246.

Crapo, R. O., R. Casaburi, A. L. Coates, P. L. Enright, J. L. Hankinson, C. G. Irvin, et al. 2000. Guidelines for methacholine and exercise challenge testing-1999. This official statement of the American Thoracic Society was adopted by the ATS Board of Directors, July 1999. Am. J. Respir. Crit. Care Med. 161:309–329.

Dellaca, R. L., M. A. Olerud, E. Zannin, P. Kostic, P. P. Pompilio, G. Hedenstierna, et al. 2009. Lung recruitment assessed by total respiratory system input reactance. Intensive Care Med. 35:2164–2172.

Downie, S. R., C. M. Salome, S. Verbanck, B. Thompson, N. Berend, and G. G. King. 2007. Ventilation heterogeneity is a major determinant of airway hyperresponsiveness in asthma, independent of airway inflammation. Thorax 62:684–689.

Hogg, J. C., F. Chu, S. Utokaparch, R. Woods, W. M. Elliott, L. Buzatu, et al. 2004. The nature of small-airway obstruction in chronic obstructive pulmonary disease. N. Engl. J. Med. 350:2645–2653.

Kaczka, D. W., E. P. Ingenito, E. Isreal, and K. R. Lutchen. 1999. Airway and Lung Tissue Mechanics in Asthma. Am. J. Respir. Crit. Care Med. 159:169–178.

Kaczka, D. W., C. B. Massa, and B. A. Simon. 2007. Reliability of estimating stochastic lung tissue heterogeneity from pulmonary impedance spectra: a forward-inverse modeling study. Ann. Biomed. Eng. 35:1722–1738.

Kaczka, D. W., K. R. Lutchen, and Z. Hantos. 2011. Emergent behavior of regional heterogeneity in the lung and its effects on respiratory impedance. J. Appl. Physiol. 110:1473–1481.

Kirby, M., L. Mathew, A. Wheatley, G. E. Santyr, D. G. McCormack, and G. Parraga. 2010. Chronic obstructive pulmonary disease: longitudinal hyperpolarized ^{3}He MR imaging. Radiology 256:280–289.

Kirby, M., L. Mathew, M. Heydarian, R. Etemad-Rezai, D. G. McCormack, and G. Parraga. 2011. Chronic obstructive pulmonary disease: quantification of bronchodilator effects by using hyperpolarized ^{3}He MR imaging. Radiology 261:283–292.

Kirby, M., M. Heydarian, S. Svenningsen, A. Wheatley, D. G. McCormack, R. Etemad-Rezai, et al. 2012. Hyperpolarized ^{3}He magnetic resonance functional imaging semiautomated segmentation. Acad Radiol. 19:141–152.

Kirby, M., D. Pike, H. O. Coxson, D. G. McCormack, and G. Parraga. 2014. Hyperpolarized (3)he ventilation defects used to predict pulmonary exacerbations in mild to moderate chronic obstructive pulmonary disease. Radiology 273:887–896.

de Lange, E. E., J. P. III Mugler, J. R. Brookeman, J. Knight-Scott, J. D. Truwit, C. D. Teates, et al. 1999. Lung air spaces: MR imaging evaluation with hyperpolarized 3He gas. Radiology 210:851–857.

de Lange, E. E., T. A. Altes, J. T. Patrie, J. D. Gaare, J. J. Knake, J. P. Mugler, et al. 2006. Evaluation of Asthma With Hyperpolarized Helium-3 MRI: correlation With Clinical Severity and Spirometry. Chest 130:1055–1062.

de Lange, E. E., T. A. Altes, J. T. Patrie, J. Parmar, J. R. Brookeman, J. P. 3rd Mugler, et al. 2007. The variability of regional airflow obstruction within the lungs of patients with asthma: assessment with hyperpolarized helium-3 magnetic resonance imaging. J. Allergy Clin. Immunol. 119:1072–1078.

Leary, D., T. Winkler, A. Braune, and G. N. Maksym. 2014. Effects of airway tree asymmetry on the emergence and spatial persistence of ventilation defects. J. Appl. Physiol. 117:353–362.

Lutchen, K. R., and H. Gillis. 1997. Relationship between heterogeneous changes in airway morphometry and lung resistance and elastance. J. Appl. Physiol. 83:1192–1201.

Mead, J. 1979. Problems in interpreting common tests of pulmonary me-chanical function. Pp. 43–52 in P. Macklem and S. Permutt, eds. The Lung in Transition between Health and Disease. Mercel Dekker, New York.

Nagels, J., F. J. Làndsér, L. van der Linden, J. Clément, and K. P. Van de Woestijne. 1980. Mechanical properties of lungs and chest wall during spontaneous breathing. J. Appl. Physiol. 49:408–416.

Otis, A. B., C. B. McKerrow, R. A. Bartlett, J. Mead, M. B. McIlroy, N. J. Selver-Stone, et al. 1956. Mechanical factors in distribution of pulmonary ventilation. J. Appl. Physiol. 8:427–443.

Parraga, G., A. Ouriadov, A. Evans, S. McKay, W. W. Lam, A. Fenster, et al. 2007. Hyperpolarized 3He ventilation defects and apparent diffusion coefficients in chronic obstructive pulmonary disease: preliminary results at 3.0 Tesla. Invest. Radiol. 42:384–391.

Pike, D., M. Kirby, F. Guo, D. G. McCormack, and G. Parraga. 2015. Ventilation heterogeneity in ex-smokers without airflow limitation. Acad Radiol 22:1068–1078.

Samee, S., T. Altes, P. Powers, E. E. de Lange, J. Knight-Scott, G. Rakes, et al. 2003. Imaging the lungs in asthmatic patients by using hyperpolarized helium-3 magnetic resonance: assessment of response to methacholine and exercise challenge. J. Allergy Clin. Immunol. 111:1205–1211.

Svenningsen, S., M. Kirby, D. Starr, H. O. Coxson, N. A. Paterson, D. G. McCormack, et al. 2014. What are ventilation defects in asthma? Thorax 69:63–71.

Tawhai, M. H., P. Hunter, J. Tschirren, J. Reinhardt, G. McLennan, and E. A. Hoffman. 2004. CT-based geometry analysis and finite element models of the human and ovine bronchial tree. J. Appl. Physiol. 97:2310–2321.

Tawhai, M. H., M. P. Nash, C. L. Lin, and E. A. Hoffman. 2009. Supine and prone differences in regional lung density and pleural pressure gradients in the human lung with constant shape. J. Appl. Physiol. 107:912–920.

Tgavalekos, N. T., J. G. Venegas, B. Suki, and K. R. Lutchen. 2003. Relation between structure, function, and imaging in a three-dimensional model of the lung. Ann. Biomed. Eng. 31:363–373.

Tgavalekos, N. T., M. Tawhai, R. S. Harris, G. Musch, M. Vidal-Melo, J. G. Venegas, et al. 2005. Identifying airways responsible for heterogeneous ventilation and mechanical dysfunction in asthma: an image functional modeling approach. J. Appl. Physiol. 99:2388–2397.

Tgavalekos, N. T., G. Musch, and R. S. Harris. 2007. Vidal Melo MF, Winkler T, Schroeder T, Callahan R, Lutchen KR, and Venegas JG. Relationship between airway narrowing, patchy ventilation and lung mechanics in asthmatics. Eur. Respir. J. 29:1174–1181.

Venegas, J. G. W. T., and G. Musch. 2005. Vidal Melo MF, Layfield D, Tgavalekos N, Fischman AJ, Callahan RJ, Bellani G, and Harris RS. Self-organized patchiness in asthma as a prelude to catastrophic shifts. Nature 434:777–782.

Venegas, J., T. Schroeder, S. Harris, R. Winkler, and M. Melo. 2005. The distribution of ventilation during bronchoconstriction is patchy and bimodal: a PET imaging study. Respir. Physiol. Neurobiol. 148:57–64.

Verbanck, S., D. Schuermans, M. Paiva, and W. Vincken. 2003. Nonreversible conductive airway ventilation heterogeneity in mild asthma. J. Appl. Physiol. 94:1380–1386.